Available online at www.sciencedirect.com
ScienceDirect
Journal of Organometallic Chemistry 692 (2007) 4227–4236
Journal of Organometallic Chemistry
www.elsevier.com/locate/jorganchem

A possible 2,1 → 3,1 isomerization mechanism in zirconocene-catalyzed propene polymerization: An application of the density functional theory and combined ONIOM approach

Julien Pilmé [a,*], Vincenzo Busico [a], Maurizio Cossi [b], Giovanni Talarico [a]

[a] *Dipartimento di Chimica, Università di Napoli "Federico II", Via Cintia, 80126 Napoli, Italy*
[b] *Dipartimento di Scienze e Tecnologie Avanzate, Università del Piemonte Orientale, Via Bellini 25/G, 15100 Alessandria, Italy*

Received 10 May 2007; received in revised form 17 June 2007; accepted 17 June 2007
Available online 30 June 2007

Abstract

The unimolecular isomerization mechanism from a secondary 2,1 → 3,1 propene unit promoted by the prototype zirconocene system $H_2SiCp_2Zr^+(P)$ (P = polymeryl chain) has been investigated by using density functional theory calculations (B3LYP) for both gas and solvent phases. The typical route occurring through β-hydrogen elimination to the metal, olefin rotation around the metal center and olefin reinsertion into the metal hydrogen bond has been calculated by using QM/MM calculations with the ONIOM model in the presence of the counterion $CH_3B(C_6F_5)_3^-$ and compared to the alternative intramolecular reversible formation of a zirconocene allyl dihydrogen complex. Our calculations show that the alternative route remains energetically less accessible, at least for the prototype metallocene system used here.

Keywords: Density functional theory; Zirconocene-catalyzed propene polymerization; Isomerization mechanism; Allylic activation; Counterion; QM/MM; ONIOM

1. Introduction

Homogeneous metallocene-catalyzed propene polymerizations exhibit a large regioselectivity preference in favor of 1,2 (primary) monomer insertion [1–3]. Nevertheless, isolated 2,1 (secondary) propene units are clearly detectable in the polypropylene samples and produce a less of catalyst efficiency with the formation of the so-called "dormant site" (see Chart 1a) [3,4]. One way for the sterically hindered secondary M–polymeryl bond to create a much less congested structure is the isomerization of the last-inserted unit to a 3,1 enchainment with the formation of tetramethylene units [5] (see Chart 1b).

The unimolecularity of 2,1 to 3,1 isomerization mechanism has been proved experimentally [6], as the ratio of [2,1]/[3,1] follows a simple first-order dependence on monomer concentration. A possible mechanism has been proposed [5,7] (see Scheme 1).

The sequence involves several steps after the preliminary 2,1 propene insertion (a): the β-hydrogen transfer from the methyl group to the metal (b); the rotation of coordinated α-olefin around the metal center (c); and olefin reinsertion into the M–H bond leading to the final product (d).

It is worth to note that a growing-chain isomerization mechanism starting from a *primary* alkyl chain has been already computationally studied [8,9] by using gas phase calculations and without taking into account the counterion. As far as we know, computational studies focusing on the isomerization of a *secondary* growing chain and in the presence of the counterion are still missing. In this paper we try to fulfill this lack modeling the isomerization of a secondary growing chain into a 3,1 unit (see Scheme 1) by means of mixed quantum mechanics/molecular

* Corresponding author.
E-mail address: julien.pilme@univ-lyon1.fr (J. Pilmé).

0022-328X/$ - see front matter © 2007 Elsevier B.V. All rights reserved.
doi:10.1016/j.jorganchem.2007.06.048

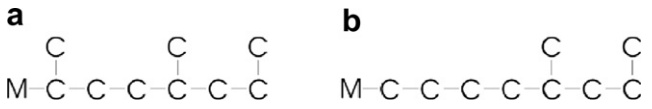

Chart 1.

mechanics (QM/MM) calculations in the presence of the counterion. This route will be also compared with an alternative mechanism based on the reversible formation of zirconocene allyl dihydrogen complexes (see Scheme 2 of Ref. [10]), which has been reported to explain the occurrence of primary growing-chain-end epimerization as well as the 2,1 → 3,1 isomerization route [10]. For the sake of readability and to compare our data with the ones already reported in the literature, we also modeled the isomerization mechanism promoted by a primary chain. The simple model precursor of catalyst, $H_2SiCp_2Zr^+$–CH_3, was chosen as prototype of the metallocene complexes, and $[(CH_3)B(C_6F_5)_3]^-$ was selected as the counterion .

2. Computational methods

Calculations have been performed at the hybrid density functional B3LYP level [11a,11b,11c] with GAUSSIAN03 program [12]. Single point calculations with BP86 [11d,11e] functional were also done for useful comparison with reported studies [8,9]. The pseudo-potential double zeta pseudo-orbital basis LANL2DZ [13] has been used for the zirconium whereas the 6-31G(2d,p) basis set has been used for the other atoms (C, H, Si, B and F). All the geometries were fully optimized without symmetry constraint. Transition state (TS) geometries were approached by a linear-transit procedure, while optimizing all other degrees of freedom. Full TS searches were started from the geometries corresponding to maxima along the linear-transit curves. Each TS displays only one negative eigenvalue according to a non-ambiguous saddle point. In order to validate the consistency of using of LanL2DZ pseudo-potential, we have completed our calculations by single point calculations with DGDZVP basis set [14] optimized for solving the Kohn-Sham equations. These all-electron calculations have confirmed our conclusions since the differences in the relative energetic values were found lower than 1 kcal/mol. QM/MM calculations were carried out at two layers following the standard ONIOM model [15,16], as displayed in Fig. 1.

Test calculations were done in order to select the suitable QM part of $[CH_3B(C_6F_5)_3]^-$ represented by

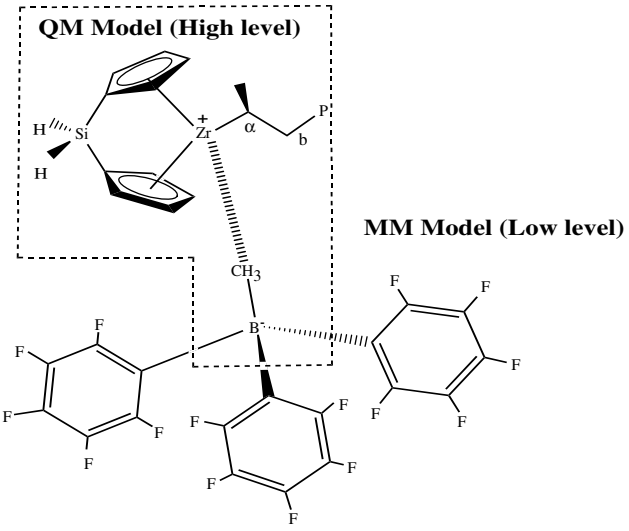

Fig. 1. QM/MM model, high and low levels.

$CH_3BCl_3^-$ and/or $CH_3BH_3^-$ [17]. In addition, representative QM/MM calculations with the counterion were also compared with the full QM calculations; in all cases the higher variation on the TS values were found lower than 2 kcal/mol, which does not modify the chemical conclusions reported here (see next sections).

The B3LYP functional was used for the high level and the standard Universal force field was used for the low layer [18]. QM/MM optimized structures of the contact ion pair [19,20] $[H_2SiCp_2ZrP]^+[(CH_3)B(C_6F_5)_3]^-$ were performed in the gas phase with only one constraint, i.e., the frozen elongation distance associated to the imaginary frequency. The solvent correction ($\varepsilon = 2.379$) was carried out by single point calculations using the optimized gas phase geometry with the conductor polarized continuum model (CPCM) [21] which is a variant of the standard polarizable continuum model (PCM) [22].

The DFT calculations have been supported by the *Quantum Theory of Atoms in Molecules* [23] (QTAIM) implemented in the TopMod program [24]. The QTAIM theory enables to provide the atomic charges following the topological approach. This method allows a partitioning of the molecular space which is achieved by the theory of dynamical systems. This partitioning gives a set of basins localized around the attractors (maxima) of the vector field of the electron density and the basins are associated to each of the atoms in the molecule. The atomic charges are calculated by integration of the electron density over the basin defining an atom.

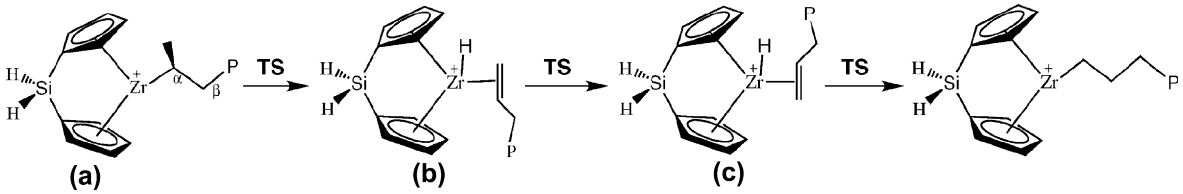

Scheme 1. Scheme for the 2,1 → 3,1 mechanism.

3. Results and discussion

Our starting point is the optimized cationic structure $H_2SiCp_2Zr^+$–CH_3 which displays a typical alkyl σ-bond [2] (2.217 Å). A weak α-agostic interaction (d_{Zr-H_α} = 2.628 Å; $d_{C_\alpha-H_\alpha}$ = 1.113) is also observed which make easier the propene insertion [2]. The propene insertion (primary or secondary) into the Zr–C_α bond was found to proceed according to the standard *Cossee* mechanism [25]. This mechanism successively involves π-complex structures ($\pi_{1,2}$ or $\pi_{2,1}$) and four center TS structures ($T_{1,2}$ or $T_{2,1}$), as displayed in Fig. 2.

In Table 1 are reported the relevant geometrical parameters of the optimized B3LYP geometries together with the relative energies for each structure. The primary insertion TS ($T_{1,2}$) leads to the typical β-agostic alkyl complex $H_2SiCp_2Zr^+$–isobutyl (^{i}Bu) whereas the secondary insertion TS ($T_{1,2}$) leads to the complex $H_2SiCp_2Zr^+$–secondary butyl (^{s}Bu).

A preference of 4.4 kcal/mol in favor of the 1,2 primary mode was calculated for both gas and solvent phases, in good agreement with previous studies [2,26a,27], arguing that the 2,1 insertion is clearly disfavored compared to the 1,2 insertion by steric interactions between the propene methyl group and the Cp rings [2,26,27]. With the formation of the cationic species $H_2SiCp_2Zr^+$–^{i}Bu (labeled Zr(*i*)) and $H_2SiCp_2Zr^+$–^{s}Bu (labeled Zr(*s*)), we can now evaluate the isomerization route starting from the primary (Section 3.1) and secondary (Section 3.2) polymer chain, respectively.

3.1. Primary isomerization route

Zr(*i*) complex can undergo the isomerization sequence as follows: β-hydrogen transfer to the metal (T_1 and product P_1), olefin rotation (P_1') and reinsertion into the M–H bond (T_2 and final product P_2). Fig. 3 shows the energetic profile of the 1,2 isomerization route and Fig. 4 displays each structure involved in the mechanism.

Table 1
Selected geometrical parameters calculated at B3LYP level for the primary and secondary propene insertion mechanism with respect to the numbering of Fig. 2

	Distances (Å)			Angle (deg)	Energies	
	ZrC_α	$C_\alpha C_1$	$C_\beta H_\beta$	$ZrC_\alpha C_1$	ΔE^a	ΔE^b
$\pi_{1,2}$	2.257	3.570		59.4	0.0	0.0
$T_{1,2}$	2.335	2.121		74.1	11.7	10.7
Zr(*i*)	2.258	1.536	1.175	86.9	−4.7	−6.5
	ZrC_α	$C_\alpha C_2$	$C_\beta H_\beta$	$ZrC_\alpha C_2$		
$\pi_{2,1}$	2.264	3.488		51.1	0.5	0.4
$T_{2,1}$	2.324	2.107		72.6	16.4	15.1
Zr(*s*)	2.271	1.535	1.179		−1.2	−3.5

[a] Relative energies (kcal/mol) in the gas phase.
[b] Relative energies (kcal/mol) in the solvent phase.

Our B3LYP calculations are reported in Table 2 and compared with the results of Prosenc et al. [8] computed with DFT calculations (BP86 functional, see Section 2) on gas phase with the complex Cp_2Zr^+(^{i}Bu). The β-elimination TS (T_1) exhibits a bond breaking with a typical C_β–H_β elongation (1.759 Å) and the H_β displays a strong anionic QTAIM charge of −0.40 (see Table 3) in favorable interaction with the cationic metal center. T_1 leads to the hydride system P_1 where a weak Zr–C_α interaction (d_{Zr-C_α} = 2.603 Å) without any agostic interactions was observed. Rotation of the olefin around the metal center (P_1' structure) was modeled by increasing the dihedral angle $ZrC_\alpha C_\beta H_\beta$. This process appears to be 1.7 kcal/mol above that of the hydride system of P_1. This can be explained by an unfavorable orientation of one methyl group of the chain observed for the P_1' structure. The final reinsertion barrier (T_2) was

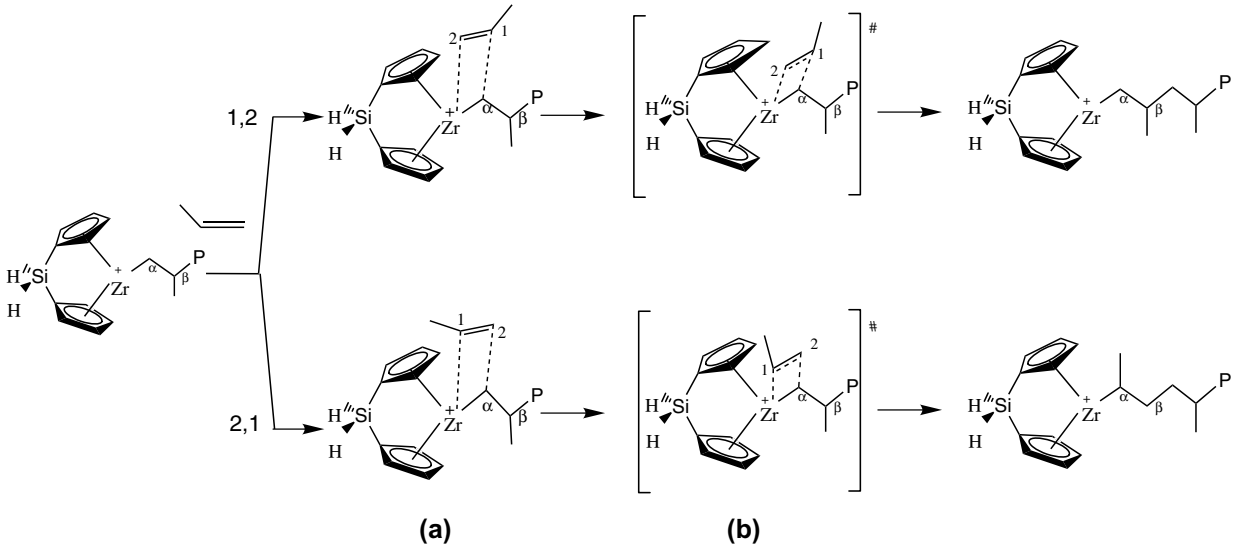

Fig. 2. Primary and secondary propene insertion at the cationic zirconocene species: (a) π complexes: $\pi_{1,2}$ (top) or $\pi_{2,1}$ (bottom); (b) transition states: $T_{1,2}$ (top) and $T_{2,1}$ (bottom).

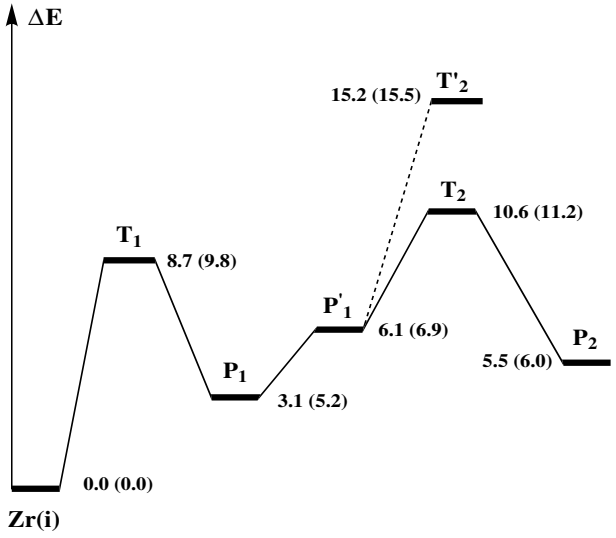

Fig. 3. Primary profile in kcal/mol. Gas phase and solvent phase (given in parenthesis). The relative position of energetic levels corresponds to the solvent corrected values.

found to be only 4.3 kcal/mol (solvent corrected) above the P'_1 structure.

An alternative route moving from the P_1 and/or the P'_1 structures is the zirconium-allyl dihydrogen formation, which, with the additional hypothesis of a reversible formation of the allyl-H complex, has been suggested [10] as a simple mechanism for primary-growing-chain-end epimerization (see Scheme 2 of Ref. [10]). We calculated the TS structure (T'_2, see Fig. 4g) leading to the stable cationic dihydrogen allyl complex (not reported here). The elongation distance C_γ–H_γ was found close to 1.46 Å and the H_β–H_γ distance of 1.034 Å (for further details see Table 3); overall, this TS is similar to the one discussed by Prosenc et al. on the unbridged Cp_2Zr–isobutyl system [8e]. Despite the fact that the charges analysis shows a favorable electrostatic configuration ($H_\beta^{-0.27}H_\gamma^{+0.07}C_\gamma^{-0.36}$), this barrier was found higher than the reinsertion barrier (T_2) by 4–5 kcal/mol both in gas and solvent phases.

It is worth to recall that calculations of the T'_2 and T_2 TS energies promoted by the complex $Cp_2Zr(^i Bu)$ were already performed by Zhu and Ziegler [8b] by using the BP86 functional. These authors calculated a preference of only 1.3 kcal/mol for the reinsertion step. In order to compare the computational approaches, we repeated our T'_2, and T_2 calculations by using the BP86 functional (see Section 2) and we found a difference of 1.4 kcal/mol. Thus, it appears that the energetic differences between these two competitive TSs is dependent of the computational method used, the BP86 value being (much) lower than the B3LYP one [9,29]. However, both methods agree in concluding that the hydrogen transfer to the metal hydride process (T'_2) appears to be less favorable than the reinsertion process (T_2).

3.2. Secondary isomerization route

The isomerization mechanism starting from Zr(*s*) shows, in principle, more alternative routes than Zr(*i*). As a matter of fact, two different β-hydrogen transfer to the metal from the alkyl complex H_2SiCp_2Zr-(^{s}Bu) are possible; they correspond, indeed, to the H-transfer coming from the methylene group (Zr)$CHCH_3$–$C\mathbf{H}_\beta H$–CH_3 and from the methyl group (Zr)CH–$C\mathbf{H}_\beta H_2$–CH_2CH_3. In Figs. 5 and 6 are reported the structures and the energetic profiles calculated, whereas in Tables 2 and 3 are listed the relevant geometrical parameters of the discussed structures as well as the QTAIM charges for each transition state involved in the mechanism. Let us examine in detail the β-hydrogen TS structures coming from the methylene (T_a, see Fig. 5b) and methyl (T_b, see Fig. 5d) groups, respectively.

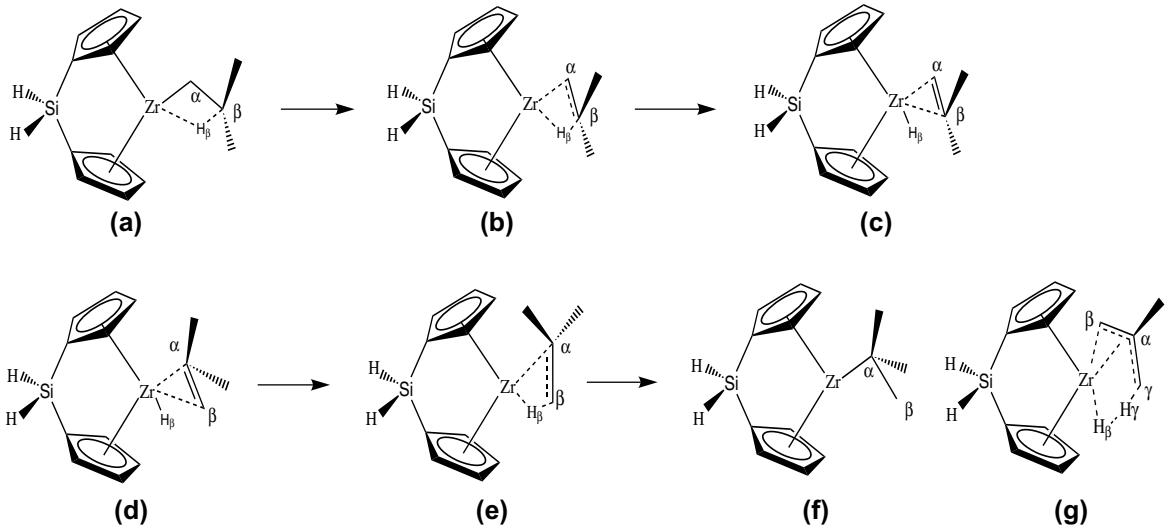

Fig. 4. Primary route. (a) Zr(*iso*-butyl); (b) T_1 β-hydrogen elimination; (c) P_1 β-elimination termination; (d) P'_1 olefin rotation; (e) T_2 reinsertion; (f) P_2 final product Zr-(*t*-butyl); (g) allylic activation TS, T'_2.

Table 2
Selected geometrical parameters calculated at B3LYP level for the primary and secondary isomerization mechanisms with respect to the numbering of Figs. 4 and 5

	Distances (Å)				Angles (deg)		Energies	
	ZrC_α	ZrH_β	$C_\beta H_\beta$	$C_\alpha C_\beta$	$ZrC_\alpha C_\beta$	$ZrC_\alpha C_\beta H_\beta$	ΔE^a	ΔE^b
Zr(*i*)	2.258	2.126	1.175	1.519	86.9	0.0	0.0 (0.0)[c]	0.0
T_1	2.409	1.869	1.759	1.407	89.2	0.0	8.7 (9.6)[c]	9.8
P_1	2.603	1.819	2.971	1.365	98.6	−1.2	3.1 (5.7)[c]	5.2
P'_1	2.777	1.810	2.532	1.356	74.6	−22.6	6.1 (6.4)[c]	6.9
T_2	2.519	1.861	1.643	1.397	76.3	−21.2	10.6 (8.8)[c]	11.2
P_2	2.308	2.117	1.162	1.508	83.2	0.1	5.5 (2.1)[c]	6.0
	ZrC_α	ZrH_β	$C_\gamma H_\gamma$	$C_\alpha C_\beta$	$H_\beta H_\gamma$	$ZrC_\alpha C_\gamma H_\gamma$		
T'_2	2.609	1.903	1.455	1.375	1.034	27.4	15.2	15.5
	ZrC_α	ZrH_β	$C_\beta H_\beta$	$C_\alpha C_\beta$	$ZrC_\alpha C_\beta$	$ZrC_\alpha C_\beta H_\beta$		
Zr(*s*)	2.271	2.162	1.154	1.512	85.3	0.1	0.0	0.0
T_a	2.434	1.854	1.685	1.395	81.7	18.1	4.4	5.5
P_a	2.616	1.812	2.709	1.355	89.7	22.6	0.2	2.0
T_b	2.462	1.855	1.744	1.385	80.0	18.9	6.2	7.6
P_b	2.659	1.817	2.468	1.353	82.6	21.3	4.2	5.7
P'_b	2.629	1.815	3.332	1.354	93.1	−27.4	4.5	6.7
T_c	2.441	1.848	1.874	1.388	87.9	−3.8	7.1	8.8
P_c	2.250	2.125	1.172	1.512	85.9	0.1	−3.9	−2.6
	ZrC_α	ZrH_β	$C_\gamma H_\gamma$	$C_\alpha C_\beta$	$H_\beta H_\gamma$	$ZrC_\alpha C_\gamma H_\gamma$		
T'_a	2.757	1.901	1.490	1.371	1.011	20.7	11.2	12.2
T'_b	2.629	1.900	1.444	1.374	1.045	21.5	13.6	14.5

[a] Relative energies (kcal/mol) in the gas phase.
[b] Relative energies (kcal/mol) in the solvent phase.
[c] In parenthesis, results from Ref. [8a].

Table 3
QTAIM charges for the transition states in the gas phase

	Zr	$q(C_\alpha)$	$q(C_\beta)$	$q(H_\beta)$	$q(C_\gamma)$	$q(H_\gamma)$
Zr(*i*)	2.35	−0.56	−0.04	−0.16	−0.03	
T_1	2.31	−0.44	−0.04	−0.40	−0.02	
T_2	2.17	−0.13	−0.20	−0.27	−0.18	
T'_2	2.19	−0.04	−0.34	−0.27	−0.36	0.07
Zr(*s*)	2.31	−0.47	−0.10	−0.14	−0.03	
T_b	2.14	−0.22	−0.19	−0.29	−0.04	
T_a	2.17	−0.24	−0.12	−0.31	−0.20	
T_c	2.27	−0.43	−0.09	−0.37	−0.01	
T'_a	2.17	−0.14	−0.32	−0.25	−0.25	0.06
T'_b	2.13	−0.16	−0.35	−0.25	−0.19	0.06

$q(A) = \overline{N}(A) - Z(A)$ where $\overline{N}(A)$ is the atomic population of the atom A.

Both T_a and T_b structures display a typical C_β–H_β elongation distance (1.685 Å for T_a and 1.744 Å for T_b). Moreover, a typical C_α–C_β distance (<1.40 Å) is observed for each TS structure which supports a partial sp^2 character for this bond. Energetically, T_a was found 1.9 kcal/mol lower than T_b both in gas and solvent phase. The lower value of T_a is a consequence of the more stable termination product P_a (hydride-zirconocene-2-butene) compared to P_b (hydride-zirconocene-1-butene) for about 3.7 kcal/mol. A QTAIM analysis confirms that T_a shows a favourable charge delocalization on three centers ($C_\alpha^{-0.24}C_\beta^{-0.12}C_\gamma^{-0.20}$) whereas T_b displays a charge delocalization on only two centers ($C_\alpha^{-0.22}C_\beta^{-0.19}$).

Because P_a is symmetrical, this isomerization way involves the same insertion/reinsertion TS leading to the initial structure Zr(*s*). In contrast, the 2,1 → 3,1 isomerization route (T_b, P_b) involves a distinct TS for the hydrogen reinsertion (T_c) after the olefin rotation around the metal center (P'_b). This rotation is characterized by the evolution of the dihedral angle $ZrC_1C_2H_2$ moving from 21.3° (P_b) to −27.4° (P'_b). The coordinated 1-butene chain can rotate to the front of the complex to avoid significant repulsive interactions with the Cp rings. A weak agostic interaction is observed for P_b and a small preference of 1 kcal/mol was found in favor of the structure of P_b (solvent phase). The final step of this 2,1 → 3,1 mechanism is the reinsertion leading to the 3,1 product (P_c). The TS of this process (T_c) exhibits a flat barrier with an energetic value slightly higher than the P'_b structure (2.1 kcal/mol in the solvent phase).

The fact that the lower β-hydrogen transfer TS corresponds to the T_a structure, which is not suitable for the classical mechanism, might trigger the alternative isomerization mechanism based on the reversible formation of zirconocene allyl dihydrogen complexes [8,10,28]. For this reason we calculated the two TS structures (T'_a and T'_b displayed in Fig. 7) corresponding to the C–H activation coming from the methylene and methyl group of a secondary growing chain, respectively. The selected geometrical parameters of the optimized geometries obtained at B3LYP/6-31G(2d,p) level together with the energetic quantities are reported in Table 2. As previously observed for

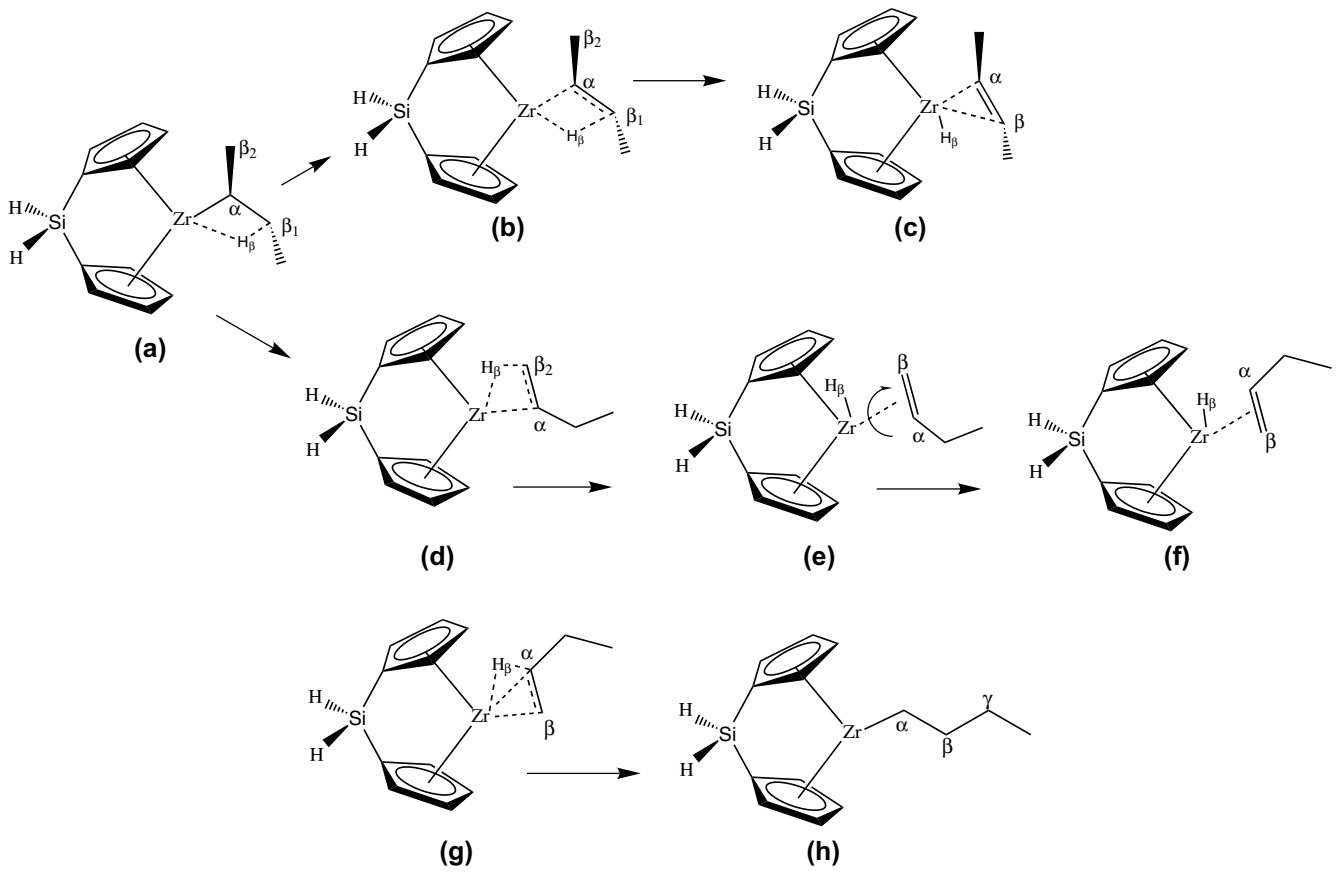

Fig. 5. Possible secondary routes. (a) Zr-(*s*-butyl); (b) T_a, β_1-elimination; (c) P_a, β_1-elimination termination; (d) T_b, β_2-elimination; (e) P_b, β_2-elimination termination; (f) P'_b, olefin rotation; (g) T_c, olefin reinsertion; (h) P_c, final 3,1 product. The 2,1 → 3,1 route involves the β_2-elimination.

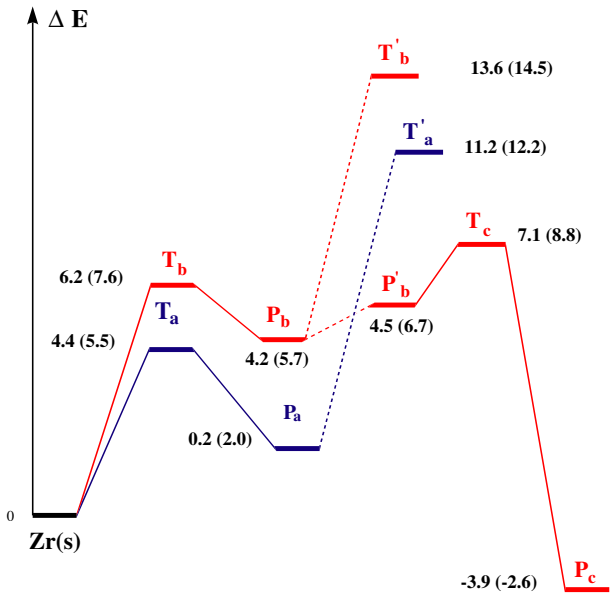

Fig. 6. Possible secondary profiles in kcal/mol. Gas phase and solvent phase (given in parenthesis). The relative position of energetic levels corresponds to the solvent corrected values.

the primary route, both transition states for the hydrogen transfer show a bond breaking with the typical C_γ–H_γ elongation ($d_{C_\gamma-H_\gamma} > 1.40$Å) and a bond forming with a small H_γ–H_β distance close to 1 Å. In addition, the charge analysis (see Table 3) reveals an electrostatic configuration of $Zr^{+2.13}H_\beta^{-0.25}H_\gamma^{+0.06}C_\gamma^{-0.19}$ for the T'_b structure. However, the energetic values for both T'_a and T'_b remain higher (>5 kcal/mol) than, respectively, T_a and T_b, in agreement with our previous conclusions on the primary route.

3.3. Counterion effects

The reaction paths reported in the previous sections were calculated on the "naked cation" although with solvent correction. However, there are several experimental [19] and theoretical papers [20] arguing that chain propagation, as well as chain terminations steps, are unlikely to involve completely separated ion pairs and that solvation effects are non-negligible.

In order to verify if the theoretical conclusions of Section 3.2 might be modified by taking into account the counterion in our calculations, we repeated the reaction path of the secondary growing chain in the presence of the typical counterion $(CH_3)B(C_6F_5)_3^-$. All the structural parameters and relative energies of the contact ion pair structures are reported in Tables 4 and 5, whereas the energetic numbers are relative to the $Zr(s)^+\cdots(CH_3)B(C_6F_5)_3^-$ specie. As shown in Table 4, the presence of the counterion modifies the geometry; the β-agostic interaction observed for the

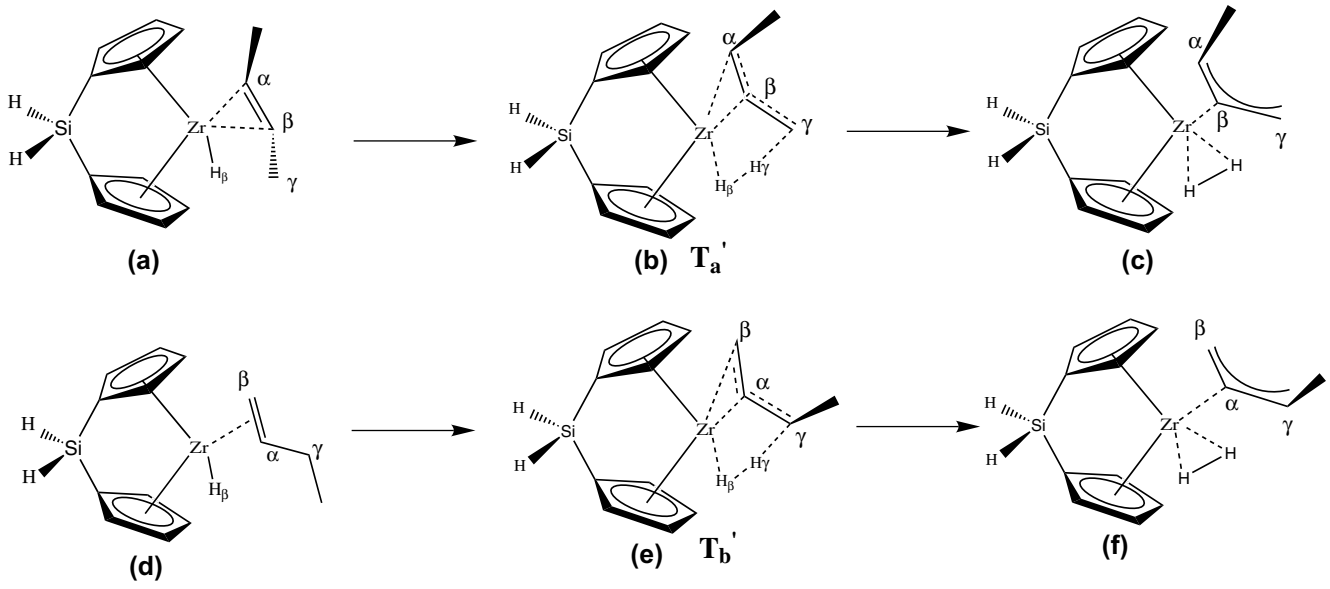

Fig. 7. Possible mechanism of allylic activation. Olefin hydrides (a) P_a and (d) P_b. TS (hydrogen transfer) (b) T'_a, (e) T'_b. Allyl dihydrogen (c) and (f).

Table 4
QM/MM optimized structural parameters of contact ion-pair with respect to the numbering of Figs. 8 and 9

	Distances (Å)								Angles (deg)				
	ZrC_a	ZrC_α	ZrC_β	ZrH_β	$C_\beta H_\beta$	$C_\alpha C_\beta$	BC_a	$H_\beta H_\gamma$	ZrC_aB	$ZrC_\alpha C_\beta$	$ZrC_\alpha C_\beta H_\beta$	$ZrC_aC_\beta H_\beta$	ΔE^a
Zr(*s*)	2.935	2.308	2.725	2.273	1.124	1.542	1.678	–	164.3	87.7	0.6	3.6	0.0
T_a	2.706	2.535	2.741	1.876	1.685	1.399	1.741	–	172.1	82.9	50.2	2.4	7.7
T_b	2.819	2.584	2.723	1.871	1.744	1.389	1.699	–	159.1	80.4	−9.0	−3.3	9.4
T_c	2.765	2.559	2.839	1.851	1.874	1.379	1.708	–	160.9	86.8	1.2	−0.5	5.2
T'_a	4.654	2.863	3.303	1.901	–	1.367	1.644	1.034	137.9	46.1	−16.6	−4.8	12.3
T'_b	4.296	3.343	2.549	1.902	–	1.371	1.651	1.045	132.2	70.9	−19.2	−4.4	15.3

[a] Relative energy (B3LYP single point obtained with the QM/MM geometry, in kcal/mol) in the solvent phase.

Table 5
Counterion effect

	Gas			Solvent		
	E^a	$E_{ionpair}{}^b$	Δ^c	E^a	$E_{ionpair}{}^b$	Δ^c
Zr(*s*)	0.0	0.0 (0.0)	0.0	0.0	0.0 (0.0)	0.0
T_a	4.4	7.2 (6.6)	2.9	5.5	7.7 (7.2)	2.2
T_b	6.2	9.1 (9.0)	2.8	7.6	9.4 (9.3)	1.8
T_c	7.1	5.5 (6.4)	−1.6	8.8	5.2 (6.2)	−3.6
T'_a	11.2	16.1 (16.5)	5.0	12.2	12.3 (12.2)	0.1
T'_b	13.6	18.0 (18.5)	4.4	14.5	15.3 (15.4)	0.8

[a] B3LYP/6-31G(2d,p) relative energies (kcal/mol) without counterion.
[b] Relative energies (B3LYP/6-31G(2d,p) single point in kcal/mol) of the contact ion-pair. In parenthesis, BP86/6-31G(2d,p) single point.
[c] $\Delta = E_{ionpair} - E$.

structure of Zr(*s*) ($d_{Zr-H_\beta} = 2.162$ Å, $d_{C\beta-H_\beta} = 1.154$ Å) is weakened in the presence of the counterion ($d_{Zr-H_\beta} = 2.273$ Å, $d_{C_\beta-H_\beta} = 1.124$) because of the formation of a contact ion pair. The charge analysis supports the view of the contact ion pair since the total charge of counterion was found of −0.8 whereas the zirconium atom keeps a strong cationic charge of 1.8.

A deeper analysis of the geometries relative to the β-hydrogen transfer T_a and T_b (see Fig. 8) reveals that the counterion effect although at a relatively short Zr–$CH_3B(C_6F_5)_3$ distance (<3.0 Å, see Table 4) is rather indiscriminate and does not largely affect the *relative* rates of the two possible transfer modes. In fact, our calculations in the gas phase demonstrated that although the gap between the initial level Zr(*s*) and the barriers T_a and T_b is approximately larger by 3 kcal/mol in presence of the counterion (Table 5) than without counterion (Table 2), however, T_a remains lower than T_b with a stable gap of 1.8 kcal/mol. Remarkably, the final reinsertion barrier T_c becomes more accessible, lower than the initial β-hydrogen elimination T_b.

Calculations in the solvent phase provide quite similar results, as well as the test calculations performed with the BP86 functional using the B3LYP geometries (see Table 5).

As a final step, let us now examine the counterion effect on the intramolecular formation of a zirconocene allyl dihydrogen complexes and in particular on the two TSs of allylic activation. In Fig. 9 are reported the geometries of both T'_a and T'_b optimized in gas phase in presence of the counterion by means of the QM/MM approach. In contrast to the β-H elimination, these TS structures show a significantly large distance μ-Zr···CH_3–B close to 4 Å

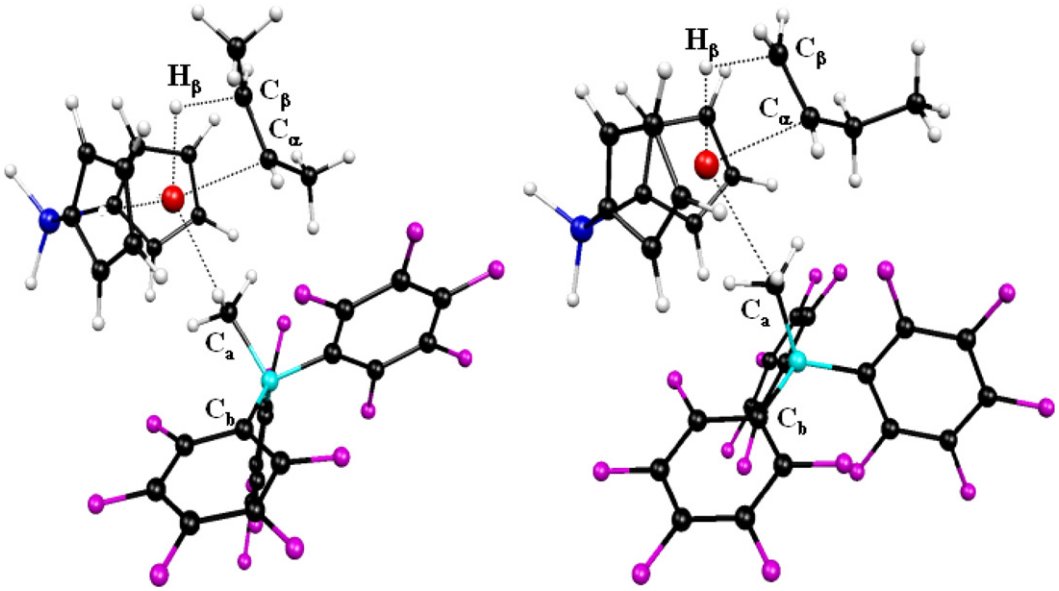

Fig. 8. Transition state structures for the β-hydrogen transfer to the metal in the presence of the counterion: T_a (left), T_b (right). Code color: Zr = red, Si = navy blue, B = light blue, F = magenta, C = black, H = white. (For interpretation of the references in color in this figure legend, the reader is referred to the web version of this article.)

(see Fig. 9), although the total charge of the counterion was found to be close to −0.8, which still supports a contact ion pair model.

The steric encumbrance in the space volume affected by the contact ion pair model provides a convincing rationale for the longer μ-Zr···CH_3–B bond of T'_a and T'_b compared to T_a and T_b, because the larger "5-center like" TS (see Fig. 9) vs. the 4-center TS (see Fig. 8) allows less room for a CH_3–$B(C_6F_5)_3^-$ approach [30]. Because of the ion pair μ-Zr···CH_3–B interaction is predominantly electrostatic in character, indeed, calculations without solvent corrections reveal that the presence of the counterion has an unfavor-

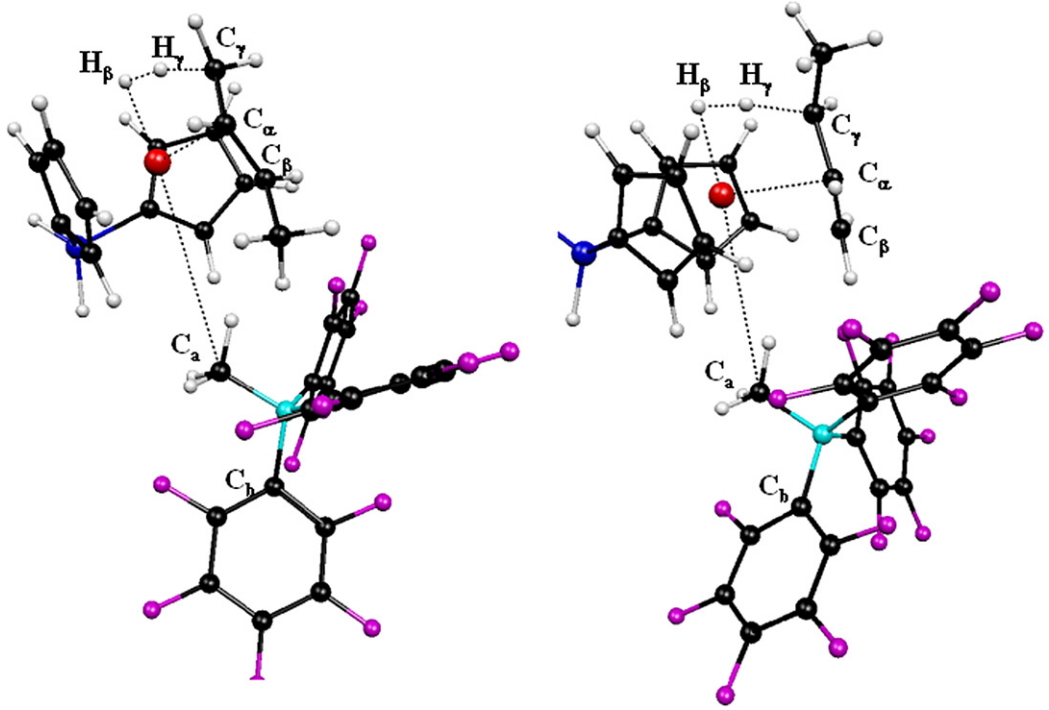

Fig. 9. Transition state structures for the intramolecular reversible formation of zirconocene allyl dihydrogen complexes in the presence of the counterion: T'_a (right), T'_b (left). Code color: Zr = red, Si = navy blue, B = light blue, F = magenta, C = black, H = white. (For interpretation of the references in color in this figure legend, the reader is referred to the web version of this article.)

able energetic effect on the allylic activation barriers (≈4–5 kcal/mol see Table 5); however, solvent corrections substantially reduce this unfavorable energetic effect to less than 1 kcal/mol.

Finally, all these results reveal that although the T'_a and T'_b barriers appear energetically accessible, the intramolecular reversible formation of a zirconocene allyl dihydrogen complexes is poorly competitive with respect to the ''classical'' isomerization route [7], at least for the model system used here.

4. Conclusions

In conclusion, in this work we studied theoretically the growing-chain isomerization reactions promoted by a prototype zirconocene system focusing on the 2,1 → 3,1 mechanism by using QM/MM calculations in the presence of the counterion. The ''classical'' mechanism starting from a M–polymeryl chain through β-hydrogen transfer from the methyl group to the metal, olefin rotation and reinsertion into the M–H bond was calculated and compared to the one based on the intramolecular reversible formation of a zirconocene allyl dihydrogen complex. Our results show a preference for the classical mechanism both for a primary and a secondary growing chain at least for the metallocene prototype system used here. Nevertheless, this alternative process is a possible competitive pathway for growing-chain isomerization in particular for the secondary growing chain.

Acknowledgements

This research was co-funded by the Italian Ministry for University (PRIN 2006). The calculations were carried out at the Centro di Metodologie Chimico-Fisiche (CIMCF), University of Naples ''Federico II''.

Appendix A. Supplementary material

Absolute energies obtained at the B3LYP/6-31G(2d,p) level; list of Cartesian coordinates for all the optimized gas phase structures discussed in the text. Supplementary data associated with this article can be found, in the online version, at doi:10.1016/j.jorganchem.2007.06.048.

References

[1] H.-H. Brintzinger, D. Fischer, R. Mülhaupt, B. Rieger, R.M. Waymouth, Angew. Chem., Int. Ed. 34 (1995) 1143.
[2] L. Resconi, L. Cavallo, A. Fait, F. Piemontesi, Chem. Rev. 100 (2000) 1253.
[3] V. Busico, R. Cipullo, Prog. Polym. Sci. 26 (2001) 443.
[4] V. Busico, R. Cipullo, V. Romanelli, S. Ronca, M. Togrou, J. Am. Chem. Soc. 127 (2005) 1608, and references therein.
[5] (a) K. Soga, T. Shiono, S. Takemura, W. Kaminsky, Makromol. Chem. Rapid Commun. 8 (1987) 305;
(b) A. Grassi, A. Zambelli, L. Resconi, E. Albizzati, R. Mazzocchi, Macromolecules 21 (1988) 617.
[6] (a) V. Busico, R. Cipullo, J.C. Chadwick, J.F. Modder, O. Sudmeijer, Macromolecules 27 (1994) 7538;
(b) L. Resconi, A. Fait, F. Piemontesi, M. Colonnesi, H. Rychlicki, R. Zeigler, Macromolecules 28 (1995) 6667.
[7] B. Rieger, X. Mu, D.T. Mallin, M.D. Rausch, J.C.W. Chien, Macromolecules 23 (1990) 3559.
[8] (a) M.H. Prosenc, H.-H. Brintzinger, Organometallics 16 (1997) 3889;
(b) C. Zhu, T. Ziegler, Inorg. Chim. Acta 345 (2003) 1;
(c) G. Moscardi, L. Resconi, L. Cavallo, Organometallics 20 (2001) 1918;
(d) L. Resconi, G. Moscardi, Polym. Prepr. 38 (1997) 832;
(e) S. Lieber, M.-H. Prosenc, H.-H. Brintzinger, Organometallics 19 (2000) 377.
[9] J.C.W. Lohrenz, M. Buhl, M. Weber, W. Thiel, J. Organomet. Chem. 592 (1999) 11.
[10] L. Resconi, J. Mol. Cat. A: Chem. 146 (1999) 167, and references therein.
[11] (a) C. Lee, W. Yang, R.G. Parr, Phys. Rev. B 37 (1988) 785;
(b) A.D. Becke, J. Chem. Phys. 98 (1993) 1372;
(c) A.D. Becke, J. Chem. Phys. 98 (1993) 5648;
(d) A.D. Becke, Phys. Rev. A 38 (1988) 3098;
(e) J.P. Perdew, Phys. Rev. B 33 (1986) 8822.
[12] M.J. Frisch, G.W. Trucks, H.B. Schlegel, G.E. Scuseria, M.A. Robb, J.R. Cheeseman, J.A. Montgomery Jr., T. Vreven, K.N. Kudin, J.C. Burant, J.M. Millam, S.S. Iyengar, J. Tomasi, V. Barone, B. Mennucci, M. Cossi, G. Scalmani, N. Rega, G.A. Petersson, H. Nakatsuji, M. Hada, M. Ehara, K. Toyota, R. Fukuda, J. Hasegawa, M. Ishida, T. Nakajima, Y. Honda, O. Kitao, H. Nakai, M. Klene, X. Li, J.E. Knox, H.P. Hratchian, J.B. Cross, V. Bakken, C. Adamo, J. Jaramillo, R. Gomperts, R.E. Stratmann, O. Yazyev, A.J. Austin, R. Cammi, C. Pomelli, J.W. Ochterski, P.Y. Ayala, K. Morokuma, G.A. Voth, P. Salvador, J.J. Dannenberg, V.G. Zakrzewski, S. Dapprich, A.D. Daniels, M.C. Strain, O. Farkas, D.K. Malick, A.D. Rabuck, K. Raghavachari, J.B. Foresman, J.V. Ortiz, Q. Cui, A.G. Baboul, S. Clifford, J. Cioslowski, B.B. Stefanov, G. Liu, A. Liashenko, P. Piskorz, I. Komaromi, R.L. Martin, D.J. Fox, T. Keith, M.A. Al-Laham, C.Y. Peng, A. Nanayakkara, M. Challacombe, P.M.W. Gill, B. Johnson, W. Chen, M.W. Wong, C. Gonzalez, J.A. Pople, GAUSSIAN03, Revision B.05, Gaussian, Inc., Pittsburgh, PA, 2003.
[13] (a) P.J. Hay, W.R. Wadt, J. Chem. Phys. 82 (1985) 270;
(b) P.J. Hay, W.R. Wadt, J. Chem. Phys. 82 (1985) 284;
(c) P.J. Hay, W.R. Wadt, J. Chem. Phys. 82 (1985) 299.
[14] N. Godbout, D.R. Salahub, J. Andzelm, E. Wimmer, Can. J. Chem. 70 (1992) 560.
[15] F. Maseras, K. Morokuma, J. Comput. Chem. 16 (1995) 1170.
[16] (a) T. Vreven, K. Morokuma, O. Farkas, H.B. Schlegel, M.J. Frisch, J. Comput. Chem. 24 (2003) 760;
(b) For ONIOM studies of organometallic reactions and homogeneous catalysis see K. Morokuma, D.G. Musaev, D.V. Khoroshun, T. Vreven, Z. Liu, M. Torrent, H. Basch, B.F. Yates, S. Mori, Abstracts of Papers, 220th ACS National Meeting, Washington, DC, United States, August 20–24, 2000.
[17] Z. Xu, K. Vanka, T. Firman, A. Michalak, E. Zurek, C. Zhu, T. Ziegler, Organometallics 21 (2002) 2444.
[18] (a) A.K. Rappé, C.J. Casewit, K.S. Colwell, W.A. Goddard III, W.M. Shiff, J. Am. Chem. Soc. 114 (1992) 10024;
(b) A.K. Rappé, W.M. Skiff, C.J. Casewit, Chem. Rev. 100 (2000) 1435.
[19] For a review on the ion-pair in the metal-catalyzed olefin polymerization see: E.Y.-X. Chen, T.J. Marks, Chem. Rev. 100 (2000) 1391.
[20] (a) For theoretical papers on the polymerization catalysis taking into account the counterion see e.g.: G. Lanza, I.L. Fragalà, T.J. Marks, Organometallics 21 (2002) 5594;
(b) G. Lanza, I.L. Fragalà, T.J. Marks, Organometallics 20 (2001) 4006;
(c) G. Lanza, I.L. Fragalà, T.J. Marks, J. Am. Chem. Soc. 122 (2000) 12764;

(d) Z. Xu, K. Vanka, T. Ziegler, Organometallics 23 (2004) 104;
(e) K. Vanka, Z. Xu, T. Ziegler, Can. J. Chem. 81 (2003) 1413;
(f) M.S.W. Chan, T. Ziegler, Organometallics 19 (2000) 5182;
(g) M.S.W. Chan, K. Vanka, C.C. Pye, T. Ziegler, Organometallics 18 (1999) 4624;
(h) I.E. Nifant'ev, L.Y. Ustynyuk, D.N. Laikov, Organometallics 20 (2001) 5375.

[21] V. Barone, M. Cossi, J. Phys. Chem. A 102 (1998) 1995.

[22] (a) M. Cossi, V. Barone, R. Cammi, J. Tomasi, Chem. Phys. Lett. 255 (1996) 327;
(b) V. Barone, M. Cossi, J. Tomasi, J. Comput. Chem. 19 (1998) 404.

[23] (a) R.F.W. Bader, Atoms in Molecules: A Quantum Theory, Oxford Univ. Press, 1990;
(b) R.F.W. Bader, C.F. Matta, F. Cortés-Guzmán, Organometallics 23 (2004) 6253.

[24] S. Noury, X. Krokidis, F. Fuster, B. Silvi, Comp. Chem. 23 (1999) 597.

[25] (a) P. Cossee, Tetrahedron Lett. 17 (1960) 12;
(b) P. Cossee, Tetrahedron Lett. 17 (1960) 17;
(c) E.J. Arlman, P. Cossee, J. Catal. 3 (1964) 99.

[26] (a) M. Borrelli, V. Busico, R. Cipullo, S. Ronca, P.H.M. Budzelaar, Macromolecules 35 (2002) 2835;
(b) G. Guerra, P. Longo, L. Cavallo, P. Corradini, L. Resconi, J. Am. Chem. Soc. 119 (1997) 4394;
(c) G. Guerra, L. Cavallo, G. Moscardi, M. Vacatello, P. Corradini, J. Am. Chem. Soc. 116 (1994) 2988.

[27] (a) A. Correa, G. Talarico, L. Cavallo, Kinet. Catal. 47 (2006) 170;
(b) A. Correa, G. Talarico, L. Cavallo, J. Organomet. Chem., in press.

[28] P. Margl, L. Deng, T. Ziegler, J. Am. Chem. Soc. 121 (1999) 154.

[29] For a comparison of the B3LYP and BP86 results in the olefin polymerization catalysis see e.g. G. Talarico, A.N.J. Blok, T.K. Woo, L. Cavallo, Organometallics 21 (2002) 4939, and Ref. [9].

[30] The picture reported here is similar to the one described by Ziegler at al. (see Ref. [20f]) comparing the μ-Zr···CH_3–B distance reported for the Zr–CH_2CH_3···$CH_3B(C_6F_5)_3$ (2.68 Å) with the one with the ethylene inserting into the Zr–CH_2CH_3 bond···$CH_3B(C_6F_5)_3$ (3.41 Å) ion-pairs, respectively.